Dalton Transactions

ROYAL SOCIETY OF CHEMISTRY

PAPER

View Article Online
View Journal | View Issue

Cite this: *Dalton Trans.*, 2025, **54**, 3759

Controlling pseudopolymorphism *via* robust and repetitive solvent-containing supramolecular interactions in urea-based isostructural coordination polymers†

Ghazale Khorshidi and Behrouz Notash *

In a systematic study, six pseudopolymorphic coordination polymers containing the ditopic 1,3-di(pyridin-4-yl)urea ligand (**4bpu**) constructed with d^{10} metal cations, possessing the formula $\{[M(4bpu)I_2]S\}_n$ [(M = Zn, Cd and Hg), (S = MeOH or EtOH)], namely **Zn-MeOH**, **Zn-EtOH**, **Cd-MeOH**, **Cd-EtOH**, **Hg-MeOH** and **Hg-EtOH** were obtained. The title compounds were characterized by single-crystal X-ray diffraction analysis (SC-XRD), elemental analysis (CHN), FT-IR spectroscopy, thermogravimetric analysis (TGA), and powder X-ray diffraction (PXRD). The diffraction studies show that these compounds are isostructural 1D zig-zag chain coordination polymers which is also confirmed using XPac 2.0.2 software and the occurrence of three- and one-dimensional (3D and 1D) isostructurality was investigated in terms of their molecular assembly in solid state structures. These comparisons were performed by extracting the dissimilarity index and stretching parameters, providing quantitative insights into the structural similarity across the pseudopolymorphic coordination polymers, which exhibit robust 3D isostructurality. Additionally, the geometry of the zig-zag chain structures was thoroughly analyzed, highlighting the subtle variations and common features that contribute to isostructurality. The supramolecular architecture of these pseudopolymorphs is stabilized by robust and repetitive hydrogen bonding motifs involving N–H···O, O–H···I and C–H···I interactions between the framework and guest solvent molecules (MeOH or EtOH). These interactions replace the commonly observed bifurcated hydrogen bonds (α-tape motif) between urea moieties, emphasizing the pivotal role of solvent molecules in controlling pseudopolymorphism and defining the final structural assembly. This detailed understanding of hydrogen bonding provides valuable insights into tailoring intermolecular interactions, enabling the design of materials with enhanced functionalities for diverse applications. A detailed investigation of urea–C=O···π_{py} interactions in urea-based compounds highlights the classification of these interactions as semilocalized (η^2-SL) based on geometric parameters and reveals their significance through crystallographic and database studies. Hirshfeld surface analysis has been performed for all compounds to determine the percentage contribution of intermolecular interactions.

Received 1st December 2024,
Accepted 9th January 2025

DOI: 10.1039/d4dt03344b

rsc.li/dalton

Introduction

The rapid progress of coordination polymers (CPs) is attributed to their construction from versatile organic linkers and metal nodes, enabling tailored assembly.[1–3] The design of functional CPs has emerged as a hot research topic, driven by the extensive range of potential applications for these compounds and their derived materials in gas storage and separation,[4,5] catalysis,[6,7] sensing,[8–10] magnetism,[11–13] bioimaging, and drug delivery.[14–16] From the crystal engineering point of view, the urea moiety as an important functional group could contribute as a donor and acceptor to form strong and directional multiple hydrogen bonds with a diverse range of organic and inorganic anions, solvents, and also the urea group (self-hydrogen bonding) which make it a potential building block for designing new supramolecular structures. A comprehensive examination of these interactions reveals that six membered cyclic $R_2^1(6)$, eight membered cyclic $R_2^2(8)$, and dis-

Department of Inorganic Chemistry, Shahid Beheshti University, 1983969411 Tehran, Iran. E-mail: b_notash@sbu.ac.ir; Fax: +98 2122431663; Tel: +98 2129904363

†Electronic supplementary information (ESI) available: Selected bond lengths and angles, PXRD pattern and TGA of compounds **Zn-MeOH**, **Zn-EtOH**, **Cd-MeOH**, **Cd-EtOH**, **Hg-MeOH**, and **Hg-EtOH**. CCDC 2391447 (**Zn-MeOH**), 2391448 (**Zn-EtOH**), 2391449 (**Cd-MeOH**), 2391450 (**Cd-EtOH**), 2391451 (**Hg-MeOH**) and 2391452 (**Hg-EtOH**). For ESI and crystallographic data in CIF or other electronic format see DOI: **https://doi.org/10.1039/d4dt03344b**

crete type D(2) H-bonding interactions are the most abundant in compounds containing the urea functional group.[17–19] The analysis of hydrogen bonding in urea-based frameworks plays a crucial role in enabling more effective and diverse applications. Hydrogen bonds provide structural flexibility and enhanced interaction capabilities with guest molecules, allowing these frameworks to achieve tailored functionalities.[17] For example, in gas adsorption, the hydrogen bonding sites improve the capture and separation of gases like SO_2 and NH_3.[20] In catalytic activities, these interactions facilitate reaction pathways by stabilizing intermediates,[21] while in sensing applications, hydrogen bonds enhance the selective recognition of specific molecules, such as heavy metals or nitroaromatic compounds.[22,23] This targeted functionality demonstrates how hydrogen bonding analysis is essential for optimizing these frameworks for practical uses across various scientific and industrial fields.[17]

The concept of "supramolecular isomerism" is an important aspect of crystal engineering because it illuminates the self-organization of supramolecular assemblies in crystalline materials.[24,25] Following a review by Moulton and Zaworotko in 2001, this term gained prominence.[26] It refers to a phenomenon similar to molecular isomerism, but occurring in more extended systems (organic or metal–organic systems), in which the building blocks are held together by non-covalent interactions such as hydrogen bonding, halogen bonding, π–π interactions and coordination bonding.[27]A variety of parameters such as the solvent system,[28–33] temperature,[34–36] pH value,[37,38] molar ratio,[39] additive,[28] ligand flexibility,[40,41] and so on, might possibly influence the construction of supramolecular isomers. It should be mentioned that the terms "supramolecular isomerism" and "polymorphism" in organic and metal–organic networks are quite similar and, in some cases, difficult to distinguish.[42–44] In this context, "polymorphism" refers to the presence of several superstructures formed from the same reactant's molecular building blocks.[26,45] The term "pseudopolymorphism" also known as "solvatomorphism" represents significant categories of supramolecular compounds, exhibiting variations in the structure concerning the number or nature of guest solvent(s).[46,47] Supramolecular isomers, on the other hand, have various network configurations or architectures that have similar chemical compositions but differ in their superstructures. Consequently, "polymorphism" or "pseudopolymorphism" might be considered sort of supramolecular isomerism because it can be explained by supramolecular interactions.[45,48] Polymorphism and pseudopolymorphism are prevalent in solid-state chemistry, especially in the pharmaceutical field, where variations in crystal forms significantly affect the material performance.[49] For active pharmaceutical ingredients (APIs), different polymorphs or solvatomorphs can exhibit unique physical and chemical properties, such as solubility, stability, and reactivity, which influence drug efficacy, bioavailability, and shelf life.[50] Understanding and characterization of solvatomorph forms are therefore essential in drug development to ensure consistent drug performance and optimize formulation conditions.[49,50] For instance, the solvatomorphs of naproxen sodium with solvents such as ethanol, *n*-propanol, isopropanol, *n*-butanol and isobutanol have been characterized, revealing that the molecular size of each solvent significantly affects the desolvation properties of each crystal form of these solvatomorphs.[51] Although non-covalent interactions are crucial in controlling pseudopolymorphism, systematic studies specifically examining their precise influence on stabilizing various pseudopolymorphic forms of inorganic systems are relatively scarce.[28,45] For example, in 1D pseudopolymorphic Cu(I) CPs synthesized through self-assembly in different solvents, supramolecular interactions such as hydrogen bonding, π–π stacking, and halogen bonding (notably $I^{-}\cdots\pi$ and $S\cdots\pi$ interactions) stabilize distinct structural conformations, highlighting their essential role in maintaining diverse pseudopolymorphic forms.[52]

One of the successful methodologies in the construction of supramolecular assemblies is isostructurality which refers to the identical or nearly identical crystal structures displayed by different chemical compounds.[53–61] The degree of similarity among crystals of small molecules can mainly be ascribed to directional interactions, which are characterized as supramolecular synthons.[62–65] There are a limited number of systematic studies on the construction of isostructural supramolecular architectures in coordination compounds using diverse building units, such as organic linkers or metal ions.[66–68] Isostructural CPs and MOFs with the same metals but distinct organic linkers are produced, allowing for a detailed examination into how different organic linkers affect sensing and gas sorption or separation capabilities.[69–72] Nevertheless, metal ions, which act as the nodes of coordination polymers, have a substantial impact on their physical and chemical properties such as catalysis[73] and gas adsorption.[74,75] The exploration and discussion of the impact of central metals on different behaviors have been limited.[76–79] To expand our understanding of the relationship between the identity of metal centers and isostructurality, the synthesis of pseudoholomorphic CPs containing ditopic urea-based linkers and different d^{10} metal ions was carried out. Among these linkers, 1,3-di(pyridin-4-yl) urea (**4bpu**) is a versatile ligand with pyridyl groups that serve as primary coordination sites, particularly for d^{10} metals like Zn^{II}, Cd^{II}, and Hg^{II}. The nitrogen atoms of the pyridyl groups strongly bind to these metals due to their lone pairs and the high Lewis acidity of metals. This ligand can act as a bridge, forming one-dimensional, two-dimensional, or three-dimensional frameworks based on the coordination geometry of the metal and reaction conditions.[17]

Herein, we report the syntheses and structural characterization of six isostructural urea-based pseudopolymorph CPs of divalent d^{10} metal ions of group 12, having the $\{[M(\mathbf{4bpu})I_2]S\}_n$ general formula: S = MeOH or EtOH, M = Zn (**Zn-MeOH** and **Zn-EtOH**), Cd (**Cd-MeOH** and **Cd-EtOH**), and Hg (**Hg-MeOH** and **Hg-EtOH**). This study allowed us to find robust and repetitive supramolecular synthons responsible for construction of MeOH and EtOH pseudopolymorphs in this family of coordination polymers.

Experimental section

Materials and instruments

All reagents and solvents were obtained from commercial sources and were used directly without further purification. The ligand 1,3-di(pyridin-4-yl)urea (**4bpu**) was synthesized following the literature procedure[80] and was characterized by (^{1}H & ^{13}C) NMR and FTIR spectroscopy (Fig. S1 and S2, ESI†). NMR spectra were recorded on a Bruker DRX-300 Avance NMR spectrometer. Infrared spectra were recorded on an MB102 Bomem spectrometer with KBr pellets in the 400–4000 cm^{-1} region. A Thermo Nicolet Nexus 470 was utilized for recording attenuated total reflectance Fourier transform infrared (ATR-FTIR) spectra in the region of 650 to 4000 cm^{-1}. Melting points were determined on an Electrothermal 9100 melting point apparatus and were uncorrected. The X-ray powder diffraction (PXRD) patterns were collected on a STADIP STOE apparatus. Elemental analyses (CHN) were performed on a Vario EL III elemental analyzer. TGA analyses were carried out using a Mettler Toledo Star SW 10.00 instrument under a flowing N_2 atmosphere at a heating rate of 10 °C min^{-1}.

Caution: Cadmium(II) and mercury(II) compounds should be handled with care due to their high toxicity.

Synthesis of pseudopolymorphic coordination polymers

{[Zn(4bpu)I$_2$]MeOH}$_n$ (Zn-MeOH). Compound **Zn-MeOH** was synthesized by treatment of the organic ligand and zinc iodide in MeOH under thermal gradient conditions (the convection technique[81]). For this purpose, 1,3-di(pyridin-4-yl)urea (**4bpu**) (0.0428 g, 0.2 mmol) and ZnI_2 (0.0638 g, 0.2 mmol) in a 1 : 1 mol ratio were placed in the main arm of a branched tube. MeOH was carefully added to fill both arms completely. The tube was sealed and the main arm was immersed in an oil bath at 60 °C while the other arm was kept at ambient temperature for several days and colorless needle shaped single crystals of **Zn-MeOH** were formed (Scheme 1). Yield: 74%. m.p: 240 °C. Elemental analysis for $C_{11}H_{10}I_2N_4OZn$: calculated: C, 24.77; H, 1.89; N, 10.50%; found: C, 23.62; H, 2.22; N, 9.95%. FTIR (KBr pellet, cm^{-1}) (Fig. S3†): 3476(w), 3373(w), 3292(w), 3091(w), 3033(w), 2360(w), 1742(m), 1589(s), 1507(s), 1431(m), 1333(m), 1288(s), 1257(w), 1180(s), 1063(m), 1024(s), 833(s), 745(w), 666(w), 552(m), 534(m), 418(w).

{[Zn(4bpu)I$_2$]EtOH}$_n$ (Zn-EtOH). The synthesis procedure and thermal gradient conditions were similar to the synthesis of **Zn-MeOH** except that EtOH was used instead of MeOH. Colorless plate shaped single crystals of **Zn-EtOH** were collected after several days (Scheme 1). Yield: 71%. m.p: 248 °C. Elemental analysis for $C_{11}H_{10}I_2N_4OZn$: calculated: C, 24.77; H, 1.89; N, 10.50%; found: C, 23.58; H, 2.28; N, 9.95%. FTIR (KBr pellet, cm^{-1}) (Fig. S4†): 3476(w), 3373(m), 3280(m), 3183(w), 3091(w), 3022(w), 2359(w), 1742(m), 1590(s), 1508(s), 1431(m), 1333(m), 1289(s), 1257(w), 1180(s), 1063(m), 1025(s), 909(w), 833(s), 745(m), 666(w), 552(w), 534(s).

{[Cd(4bpu)I$_2$]MeOH}$_n$ (Cd-MeOH). The synthesis procedure and thermal gradient conditions were similar to the synthesis of **Zn-MeOH** except that CdI_2 (0.0739 g, 0.2 mmol) was used instead of ZnI_2 (Scheme 1). After several days, colorless needle shaped single crystals of **Cd-MeOH** were collected (yield: 75%. m.p: 235 °C). Elemental analysis for $C_{11}H_{10}I_2N_4OCd$: calculated: C, 22.76; H, 1.74; N, 9.65%; found: C, 21.71; H, 2.09; N, 9.22%. FTIR (KBr pellet, cm^{-1}) (Fig. S5†): 3489(w), 3298(w), 3205(w), 3091(w), 2359(w), 1739(m), 1590(s), 1521(s), 1506(s), 1429(m), 1333(m), 1287(s), 1254(w), 1183(s), 1061(m), 1017(s), 960(w), 910(w), 830(s), 744(m), 659(w), 545(m), 534(s).

{[Cd(4bpu)I$_2$]EtOH}$_n$ (Cd-EtOH). Under the same thermal gradient conditions, colorless needle shaped single crystals of **Cd-EtOH** were collected (Scheme 1). The procedure was similar to the synthesis of **Cd-MeOH** except that EtOH was used instead of MeOH. After several days, colorless needle shaped single crystals of **Cd-EtOH** were collected (yield: 74%. m.p:

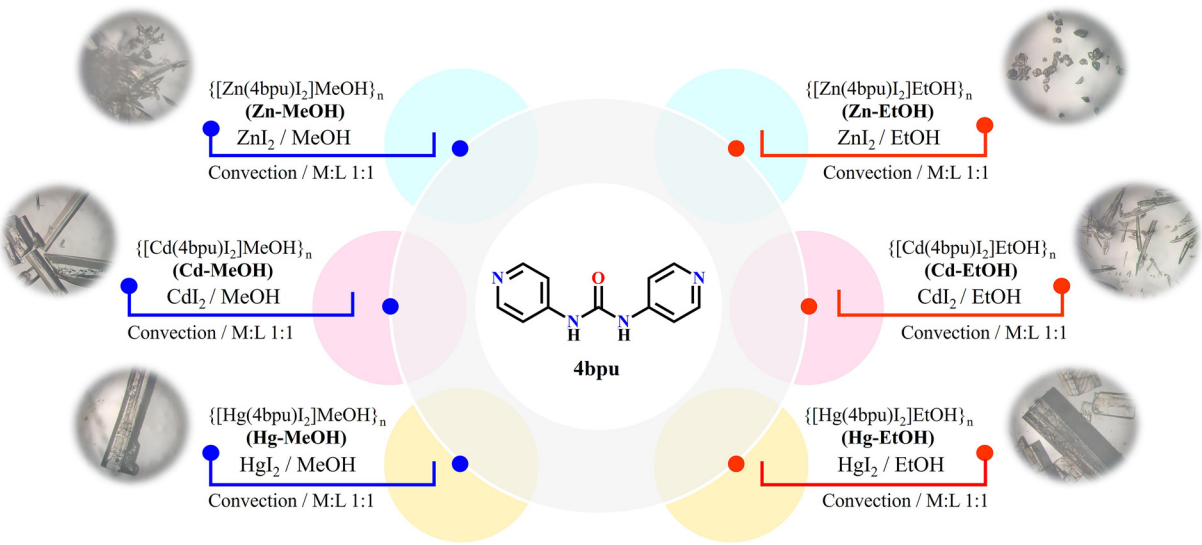

Scheme 1 Synthesis method and optical microscopic images of compounds **M-MeOH** and **M-EtOH** (M = Zn, Cd and Hg).

242 °C). Elemental analysis for $C_{11}H_{10}I_2N_4OCd$: calculated: C, 22.76; H, 1.74; N, 9.65%; found: C, 21.68; H, 2.09; N, 9.22%. FTIR (KBr pellet, cm^{-1}) (Fig. S6†): 3307(w), 3200(w), 3091(w), 1741(w), 1711(m), 1588(s), 1517(s), 1430(m), 1334(m), 1291(m), 1251(w), 1187(s), 1062(w), 1016(m), 830(s), 743(w), 668(w), 658(w), 586(w), 544(w), 530(s).

{[Hg(4bpu)I_2]MeOH}$_n$ (Hg-MeOH). The synthesis procedure and thermal gradient conditions were similar to the synthesis of **Zn-MeOH** except that HgI_2 (0.073 g, 0.2 mmol) was used instead of ZnI_2 (Scheme 1). After several days, colorless needle shaped single crystals of **Hg-MeOH** were collected (yield: 73%. m.p: 215 °C). Elemental analysis for $C_{11}H_{10}I_2N_4OHg$: calculated: C, 19.76; H, 1.51; N, 8.38%; found: C, 18.79; H, 1.80; N, 8.03%. FTIR (KBr pellet, cm^{-1}) (Fig. S7†): 3497(w), 3359(w), 3326(w), 3192(w), 3101(w), 3051(w), 3017(w), 1941(w), 1837(w), 1735(s), 1691(s), 1593(m), 1526(m), 1424(m), 1362(w), 1330(m), 1284(m), 1253(w), 1239(w), 1177(m), 1061(m), 1009(s), 908(w), 861(m), 827(s), 797(w), 744(m), 730(w), 688(m), 650(m), 531(s).

Table 1 Crystallographic and structure refinement data for compounds **M-MeOH** and **M-EtOH** (M = Zn, Cd and Hg)

	Zn-MeOH	Zn-EtOH	Cd-MeOH	Cd-EtOH	Hg-MeOH	Hg-EtOH
Formula	$C_{12}H_{14}I_2N_4O_2Zn$	$C_{13}H_{16}I_2N_4O_2Zn$	$C_{12}H_{14}I_2N_4O_2Cd$	$C_{13}H_{16}I_2N_4O_2Cd$	$C_{12}H_{14}I_2N_4O_2Hg$	$C_{13}H_{16}I_2N_4O_2Hg$
Formula weight	565.46	579.49	612.47	626.51	700.66	714.69
Crystal color, habit	Colorless, needle	Colorless, plate	Colorless, needle	Colorless, needle	Colorless, needle	Colorless, needle
T (K)	298(2)	298(2)	298(2)	298(2)	298(2)	298(2)
λ (Å)	0.71073	0.71073	0.71073	0.71073	0.71073	0.71073
Crystal system	Orthorhombic	Orthorhombic	Orthorhombic	Orthorhombic	Orthorhombic	Orthorhombic
Space group	$Pna2_1$	$Pna2_1$	$Pna2_1$	$Pna2_1$	$Pna2_1$	$Pna2_1$
Crystal size (mm)	0.50 × 0.20 × 0.20	0.25 × 0.20 × 0.10	0.30 × 0.20 × 0.15	0.30 × 0.20 × 0.10	0.20 × 0.15 × 0.10	0.25 × 0.15 × 0.10
a (Å)	9.1201(18)	8.9539(18)	9.1508(18)	9.0475(18)	9.1437(18)	9.0388(18)
b (Å)	10.018(2)	10.616(2)	10.063(2)	10.378(2)	10.043(2)	10.366(2)
c (Å)	19.490(4)	19.707(4)	19.884(4)	20.096(4)	19.926(4)	20.154(4)
V (Å^3)	1780.8(6)	1873.2(6)	1831.0(6)	1886.9(6)	1829.8(6)	1888.5(7)
Z	4	4	4	4	4	4
$D_{calc.}$ (g cm^{-1})	2.109	2.055	2.222	2.205	2.543	2.514
θ_{min}, θ_{max} (°)	2.286–24.977	2.179–24.999	2.268–24.996	2.209–24.998	2.271–24.996	2.021–24.494
F_{000}	1064	1096	1136	1168	1264	1296
μ (mm^{-1})	4.854	4.617	4.572	4.440	11.794	11.430
Index ranges	$-9 \le h \le 10$ $-11 \le k \le 11$ $-23 \le l \le 20$	$-10 \le h \le 9$ $-12 \le k \le 11$ $-23 \le l \le 20$	$-9 \le h \le 10$ $-11 \le k \le 10$ $-20 \le l \le 23$	$-9 \le h \le 10$ $-12 \le k \le 10$ $-23 \le l \le 20$	$-9 \le h \le 10$ $-11 \le k \le 10$ $-23 \le l \le 20$	$-10 \le h \le 9$ $-10 \le k \le 12$ $-20 \le l \le 23$
Data collected	5320	5358	5229	5383	5204	5218
Unique data, (R_{int})	2699, (0.1182)	3064, (0.1101)	2852, (0.0858)	3054, (0.0902)	2987, (0.1319)	2940, (0.1214)
R_1[a], wR_2[b] ($I > 2\sigma(I)$)	0.0681, 0.1642	0.0689, 0.1599	0.0589, 0.1330	0.0604, 0.1387	0.0777, 0.1576	0.0648, 0.1300
R_1[a], wR_2[b] (all data)	0.0888, 0.1757	0.1084, 0.1766	0.0826, 0.1445	0.0865, 0.1500	0.1596, 0.1946	0.1461, 0.1596
GOF on F^2 (S)	0.974	0.979	0.886	0.918	0.916	0.895
Largest diff. peak, hole (e Å^{-3})	0.971, −1.278	0.813, −0.572	1.071, −1.357	0.864, −0.661	1.335, −0.842	0.980, −1.179
CCDC No.	2391447	2391448	2391449	2391450	2391451	2391452

[a] $R_1 = \sum||F_o| - |F_c||/\sum|F_o|$. [b] $wR_2 = [\sum(w(F_o^2 - F_c^2)^2)/\sum w(F_o^2)^2]^{1/2}$.

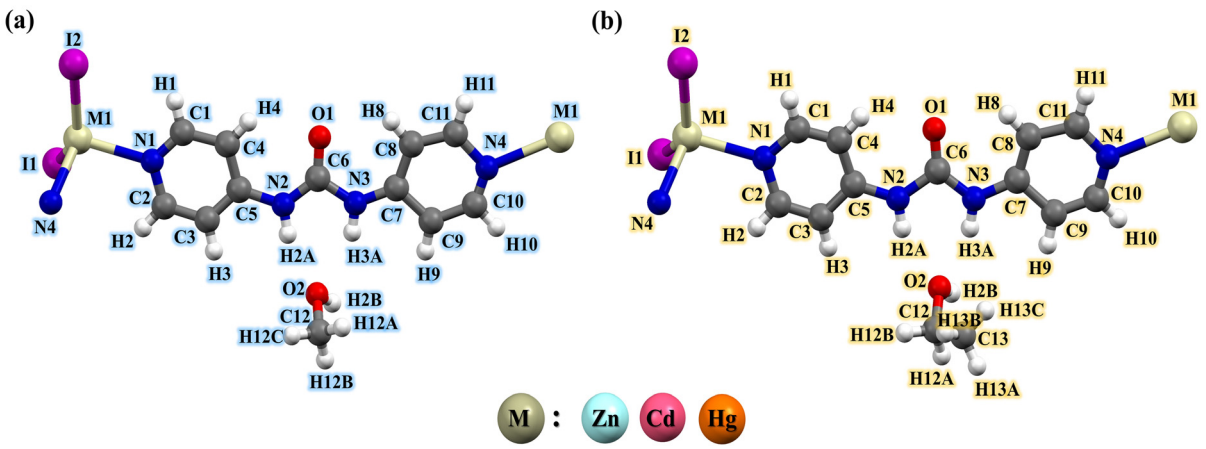

Fig. 1 View of the coordination environment around the metal center with the atom labeling scheme in (a) compounds **Zn-MeOH**, **Cd-MeOH** and **Hg-MeOH** and (b) compounds **Zn-EtOH**, **Cd-EtOH** and **Hg-EtOH**. Color code: metal (M), beige; O, red; N, blue; C, grey; I, purple and H, white.

{[Hg(4bpu)I_2]EtOH}$_n$ (Hg-EtOH). The synthesis and thermal gradient conditions were the same as those for **Hg-MeOH** except that EtOH was used instead of MeOH (Scheme 1). After several days, colorless needle shaped single crystals of **Hg-EtOH** were collected (yield: 71%. m.p: 220 °C). Elemental analysis for $C_{11}H_{10}I_2N_4OHg$: calculated: C, 19.76; H, 1.51; N, 8.38%; found: C, 18.82; H, 2.00; N, 8.03%. IR (KBr pellet, cm^{-1}) (Fig. S8†): 3523(w), 3359(w), 3326(w), 3304(w), 3206(w), 3114(w), 3045(w), 1942(w), 1837(w), 1735(s), 1691(s), 1596(s), 1526(m), 1425(m), 1363(w), 1330(m), 1284(m), 1253(w), 1233(w), 1176(m), 1085(w), 1061(m), 1009(s), 908(w), 855(m), 827(s), 797(m), 745(m), 727(m), 689(m), 650(m), 530(s).

Single-crystal X-ray diffraction studies

Details of the crystal structure determination for **M-MeOH** and **M-EtOH** (M = Zn, Cd and Hg) are presented in the ESI.† The crystal data and refinement details for all compounds are summarized in Table 1. The selected bond distances and angles for all compounds are given in Table S1.†

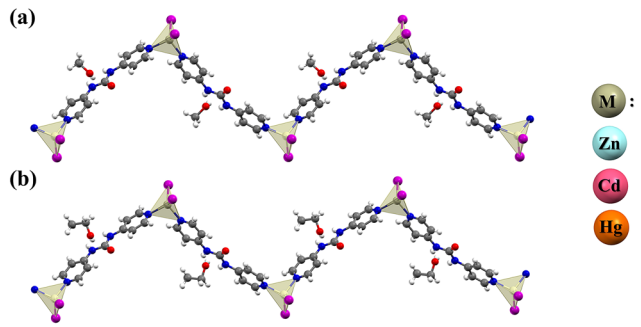

Fig. 2 A section of the 1D chain structure of (a) compounds **M-MeOH** (M = Zn, Cd and Hg) and (b) compounds **M-EtOH** (M = Zn, Cd and Hg). Metal polyhedra are shown in light beige for the metal coordination environment.

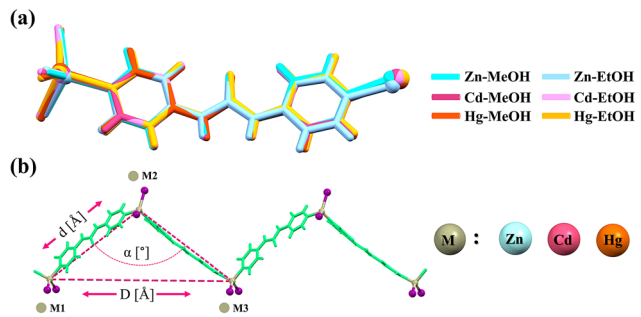

Fig. 3 (a) Structural overlay image of ligands in **M-MeOH** and **M-EtOH** (M = Zn, Cd and Hg). Metal ions are shown as balls. (b) M···M distances (*D*, *d*/Å) and M···M···M angles (α/°) in zig-zag chains.

Results and discussion

Synthesis

The **4bpu** ligand was prepared by using the reported method[80] and confirmed by spectroscopic methods. All coordination polymers were prepared in high yield by the self-assembly process of **4bup** and MI_2 (M = Zn, Cd and Hg) at a mole ratio of 1 : 1 under thermal gradient conditions (convection technique). Distinguishingly, the single crystals of these compounds were obtained from the MeOH or EtOH solvent system during the synthesis procedure (Scheme 1).

Structural description of isostructural pseudopolymorph CPs

The main skeleton of all six synthesized **M-MeOH** and **M-EtOH** (M = Zn, Cd and Hg) compounds were the same and isostructural with the orthorhombic $Pna2_1$ space group. So, the structures of **Zn-MeOH** and **Zn-EtOH** are discussed as representatives. The structures of **Cd-MeOH**, **Cd-EtOH**, **Hg-MeOH** and **Hg-EtOH** will not be described in detail. Fig. S9† depicts the ORTEP diagram and atomic labeling of all compounds and details of crystallographic data and parameters are given in Table 1. Unfortunately, despite many efforts, we were unable to grow higher quality crystals of these compounds and this was the highest resolution possible from the available data (Fig. S10–S12†).

The asymmetric unit of **Zn-MeOH** and **Zn-EtOH** contained one Zn^{II} ion, one **4bpu** ligand, two coordinated iodide anions and one MeOH molecule for **Zn-MeOH**, as well as one EtOH molecule for **Zn-EtOH** (Fig. 1 and Fig. S9†). Each Zn^{II} center is four-coordinate with two nitrogen atoms from two different **4bpu** ligands and two iodide anions in **Zn-MeOH** and **Zn-EtOH**.

The geometry of the four-coordinate metal centers can be described by an angular index (τ_4) parameter, which was defined by Houser and co-workers as follows (eqn (1)):

$$\tau_4 = \frac{360° - (\alpha + \beta)}{141°} \quad (1)$$

where α and β are the two largest angles around a four-coordinate metal center. A τ_4 value of 0 would correspond to a square planar geometry, τ_4 values of 0.07, 0.18, 0.5 and 0.64 correspond to a seesaw geometry, a τ_4 value of 0.85 corresponds to a trigonal pyramidal geometry, and a τ_4 value of 1 corresponds to a tetrahedral geometry.[82] These isostructural CPs have dis-

Table 2 Geometric characteristics for zig-zag chains of **M-MeOH** and **M-EtOH** (M = Zn, Cd and Hg)

	Zn-MeOH	Zn-EtOH	Cd-MeOH	Cd-EtOH	Hg-MeOH	Hg-EtOH
M1···M2, *d* [Å]	14.145	14.221	14.542	14.595	14.760	14.804
M1···M3 (length of the zig-zag chain period), *D* [Å]	21.914	22.384	22.285	22.618	22.314	22.664
M1···M2···M3 angle, α [°]	101.55	103.82	100.03	101.58	98.21	99.90

torted trigonal-pyramidal coordination geometry around Zn^{II}, Cd^{II} and Hg^{II} metal centers. Geometry and angular parameter τ_4 for all compounds are listed in Table S2.† The Zn–N/I, Cd–N/I and Hg–N/I bond lengths (Table S1, ESI†) are all located in the normal accepted range of Zn^{II}, Cd^{II} and Hg^{II} coordination compounds, respectively.[30,83–86] The molecular geometry of the **4bpu** ligand is found to be slightly nonplanar in all compounds, as evident from the corresponding dihedral angles involving pyridyl-urea and pyridyl–pyridyl planes (Fig. S13, ESI†). In **Zn-MeOH** and **Zn-EtOH** the ligand displayed nonplanarity with the dihedral angles of 6.29 and 6.64° involving py1-urea planes, dihedral angles of 5.37 and 5.63° involving py2-urea planes and dihedral angles of 7.67 and 9.25° involving the terminal pyridyl rings, respectively.

In all compounds, each **4bpu** links two metal (M) centers to afford an M_2L unit that propagates into a one-dimensional

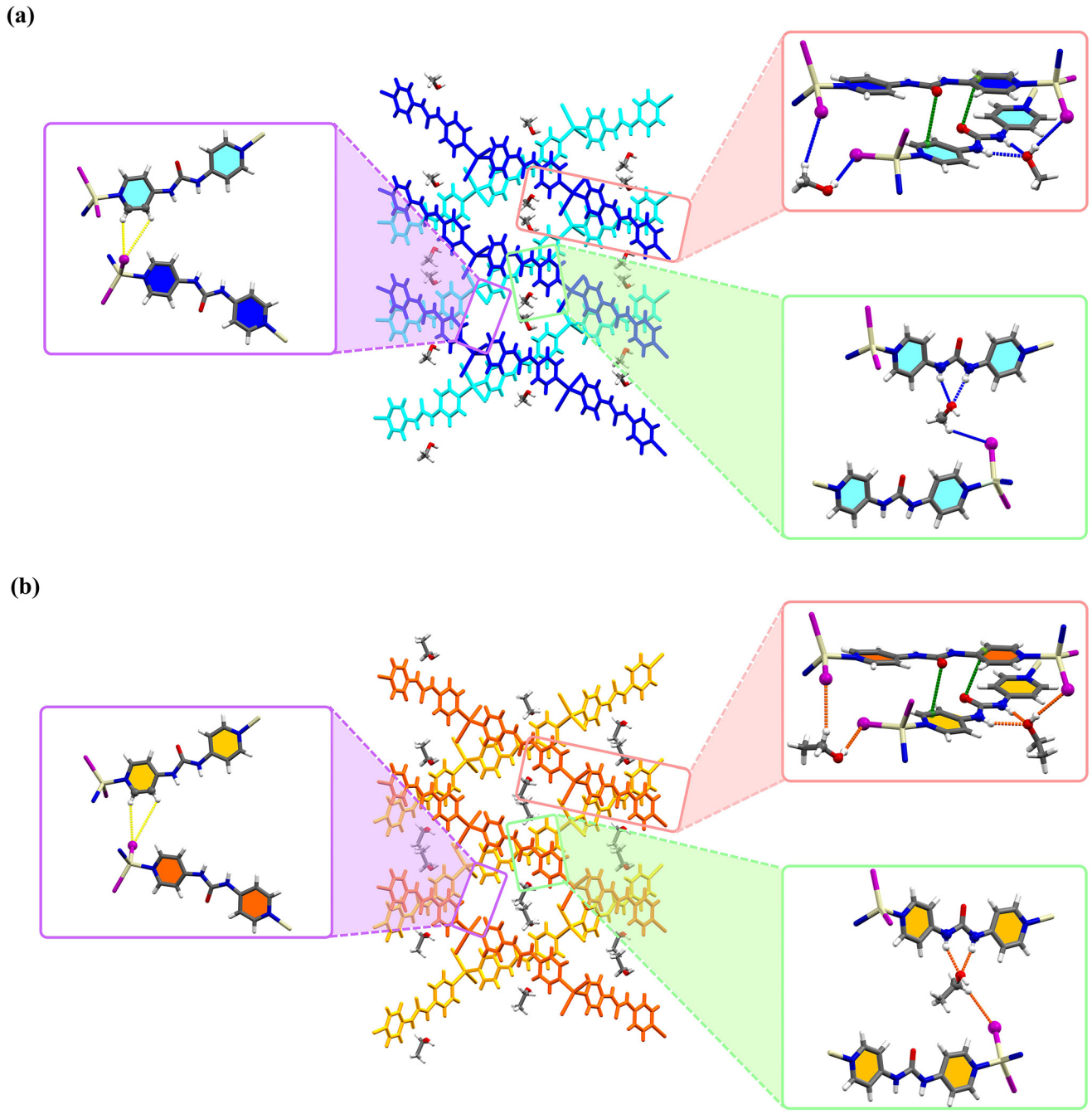

Fig. 4 The 2D supramolecular layer assembled by hydrogen bond and lone pair–π interactions. These interactions are represented by yellow and green dashed lines. Blue and orange dashed lines denote hydrogen bonds between the MeOH/EtOH and the framework in (a) compounds **Zn-MeOH**, **Cd-MeOH** and **Hg-MeOH** and (b) compounds **Zn-EtOH**, **Cd-EtOH** and **Hg-EtOH**.

Table 3 Geometry of hydrogen bonds (D–H···A) for **Zn-MeOH** and **Zn-EtOH**

Compounds	D–H···A	*d*(D–H)/Å	*d*(H···A)/Å	*d*(D···A)/Å	∠D–H···A/°
Zn-MeOH	N2–H2A···O2$^{\#1}$	0.78(7)	2.20(13)	2.93(4)	157(16)
	N3–H3A···O2$^{\#1}$	0.78(4)	2.09(5)	2.84(4)	163(6)
	O2–H2B$^{\#1}$···I2$^{\#2}$	0.78(6)	2.78(5)	3.56(3)	175(9)
	C12–H12A$^{\#1}$···I2$^{\#3}$	0.96	3.40	4.17	138.2
	C2–H2···I1$^{\#4}$	0.93	3.96	3.15	146.9
	C3–H3···I1$^{\#4}$	0.93	3.79	4.27	115.3
	C4–H4···O1	0.93	2.23	2.82(3)	121.0
	C8–H8···O1	0.93	2.24	2.82(3)	120.0
Symmetry codes: #1: $x, y-1, z-1$; #2: $-x+1, -y, z-1/2$; #3: $-x+1/2, y-1/2, z-1/2$; #4: $x-1/2, -y-1/2, z$					
Zn-EtOH	N2–H2A···O2$^{\#1}$	0.86	2.21	2.99(4)	151.0
	N3–H3A···O2$^{\#1}$	0.86	2.02	2.85(4)	160.0
	O2–H2B$^{\#1}$···I2$^{\#2}$	0.9(4)	2.7(4)	3.56(3)	169.0
	C12–H12B···I2$^{\#3}$	0.97	3.18	4.07	153.5
	C2–H2···I1$^{\#4}$	0.93	3.47	4.32	151.8
	C3–H3···I1$^{\#4}$	0.92	4.28	4.72	112.7
	C4–H4···O1	0.93	2.22	2.82(3)	122.0
	C8–H8···O1	0.93	2.30	2.87(3)	119.0
Symmetry codes: #1: $x+1/2, -y+1/2, z+1$; #2: $-x+1, -y, z+1/2$; #3: $-x+3/2, y-1/2, z+1/2$; #4: $x+1/2, -y-1/2, z$					

Table 4 Geometry of hydrogen bonds (D–H···A) for **Cd-MeOH** and **Cd-EtOH**

Compounds	D–H···A	*d*(D–H)/Å	*d*(H···A)/Å	*d*(D···A)/Å	∠D–H···A/°
Cd-MeOH	N2–H2A···O2	0.86	2.16	2.96(4)	154.0
	N3–H3A···O2	0.86	2.11	2.94(4)	160.0
	O2–H2B···I2$^{\#1}$	0.9(2)	2.7(3)	3.61(3)	170.0
	C12–H12A···I2$^{\#2}$	0.96	3.46	4.24	140.2
	C2–H2···I1$^{\#3}$	0.93	3.12	3.96	150.7
	C3–H3···I1$^{\#3}$	0.92	3.87	4.33	114.2
	C4–H4···O1	0.93	2.22	2.82(3)	121.0
	C8–H8···O1	0.93	2.22	2.82	121.0
Symmetry codes: #1: $-x+1, -y+1, z+1/2$; #2: $-x+3/2, y-1/2, z+1/2$; #3: $x+1/2, -y+1/2, z$					
Cd-EtOH	N2–H2A···O2$^{\#1}$	0.86	2.18	2.98(3)	153.0
	N3–H3A···O2$^{\#1}$	0.86	2.10	2.92(3)	159.0
	O2–H2B$^{\#1}$···I2$^{\#2}$	0.86(7)	2.77(7)	3.61(2)	164(7)
	C12–H12B$^{\#1}$···I2$^{\#3}$	0.97	3.53	4.18	126.3
	C2–H2···I1$^{\#4}$	0.92	3.27	4.13	153.7
	C3–H3···I1$^{\#4}$	0.93	4.10	4.54	112.4
	C4–H4···O1	0.93	2.25	2.83(3)	120.0
	C8–H8···O1	0.93	2.18	2.80(3)	123.0
Symmetry codes: #1: $x, y-1, z+1$; #2: $-x, -y, z+1/2$; #3: $-x+1/2, y-1/2, z+1/2$; #4: $x+1/2, -y-1/2, z$					

Table 5 Geometry of hydrogen bonds (D–H···A) for **Hg-MeOH** and **Hg-EtOH**

Compounds	D–H···A	*d*(D–H)/Å	*d*(H···A)/Å	*d*(D···A)/Å	∠D–H···A/°
Hg-MeOH	N2–H2A···O2	0.86	2.09	2.90(7)	157.0
	N3–H3A···O2	0.86	2.17	2.98(7)	156.1
	O2–H2B···I2$^{\#1}$	0.87(3)	2.86(15)	3.65(5)	151(25)
	C12–H12B···I2$^{\#2}$	0.95	3.78	4.24	111.9
	C2–H2···I1$^{\#3}$	0.92	3.14	3.95	147.0
	C3–H3···I1$^{\#3}$	0.92	3.82	4.30	115.6
	C4–H4···O1	0.93	2.24	2.83(6)	120.6
	C8–H8···O1	0.93	2.27	2.82(6)	117.0
Symmetry codes: #1: $-x+1, -y+1, z+1/2$; #2: $-x+1/2, y-1/2, z+1/2$; #3: $x-1/2, -y+1/2, z$					
Hg-EtOH	N2–H2A···O2$^{\#1}$	0.86	2.20	3.00(6)	153.0
	N3–H3A···O2$^{\#1}$	0.86	2.04	2.86(7)	160.0
	O2–H2B$^{\#1}$···I2$^{\#2}$	0.9(4)	2.9(4)	3.66(4)	158.0
	C12–H12A$^{\#1}$···I2$^{\#3}$	0.97	3.75	4.26	115.1
	C2–H2···I1$^{\#4}$	0.92	3.28	4.13	153.4
	C3–H3···I1$^{\#4}$	0.92	4.03	4.48	113.3
	C4–H4···O1	0.93	2.25	2.86(5)	122.0
	C8–H8···O1	0.93	2.25	2.84(5)	121.0
Symmetry codes: #1: $x, y, z+1$; #2: $-x+1, -y+1, z+1/2$; #3: $-x+3/2, y+1/2, z+1/2$; #4: $x+1/2, -y+3/2, z$					

(1D) zig-zag chain in which the distance between two adjacent Zn^{II} ions is 14.145 and 14.221 Å for **Zn-MeOH** and **Zn-EtOH**, respectively (Fig. 2, Fig. S14 and S15†).

Comparing overlay images of these isostructural compounds, subtle differences in atomic positions, bond lengths, and dihedral angles become apparent. Understanding these distinctions is crucial for comprehending the implications of chemical substitutions in crystal structures (Fig. 3a). In all compounds, the formed 1D zig-zag chains can be described by the M···M distances and M···M···M angles (Fig. 3b, Fig. S14, S15 ESI,† and Table 2). The values in Table 2 show how close are architectures of the one-dimensional zig-zag chains in all cases.

Interestingly, the typical bifurcated hydrogen bonding interaction between urea moieties (interaction between the carbonyl oxygen atom and the two N–H of the adjacent urea groups) that lead to the formation of 1D hydrogen bonded α-tape motif was absent in these structures. Instead, in a competition between the common α-tape hydrogen bonding and the interaction with the molecules of the alcoholic solvents used, the 1D chains are connected by the hydrogen bonding of the urea group with the guest solvents MeOH or EtOH molecules. As illustrated in Fig. 4, one such a connection is built by a set of bifurcated N–H···O and one C–H···I hydrogen bonded paths: ~(ligand)N–H···O(MeOH or EtOH)C–H···I($M^{II}IN_2$)~. According to graph set notation[87,88] this sequence can be written as $R_2^1(6)$ D(2). In these supramolecular structures, the oxygen atom (O2) of MeOH and EtOH guest molecules and also coordinated iodide anions (I1) act as bifurcated hydrogen bond acceptors. In summary, (aromatic)C–H···I, (MeOH or EtOH)C–H···I, (MeOH or EtOH)O–H···I hydrogen bonds and also urea–C═O···π_{py} play a crucial role in the crystal packing of these pseudopolymorphs. There are two intramolecular C–H···O hydrogen bonding interactions in **4bpu** ligands. A more detailed description of the hydrogen bond interactions for **Zn-MeOH**/**Zn-EtOH**, **Cd-MeOH**/**Cd-EtOH** and **Hg-MeOH**/**Hg-EtOH** is provided in Tables 3–5 and Fig. S16 and S17,† respectively.

Scheme 2 illustrates the geometric parameters of urea–C═O···π_{py} interactions and provides an overview of the classified lone pair–π interactions as localized (η^1), semilocalized (η^2) and delocalized (η^6).[89] In the case of Cg(1) and Cg(2) in all titled compounds, according to the urea–C═O···π_{py} geometric parameters (Table 6), particularly the *r* value which is slightly longer than the sum of the Bondi's van der Waals radii of the

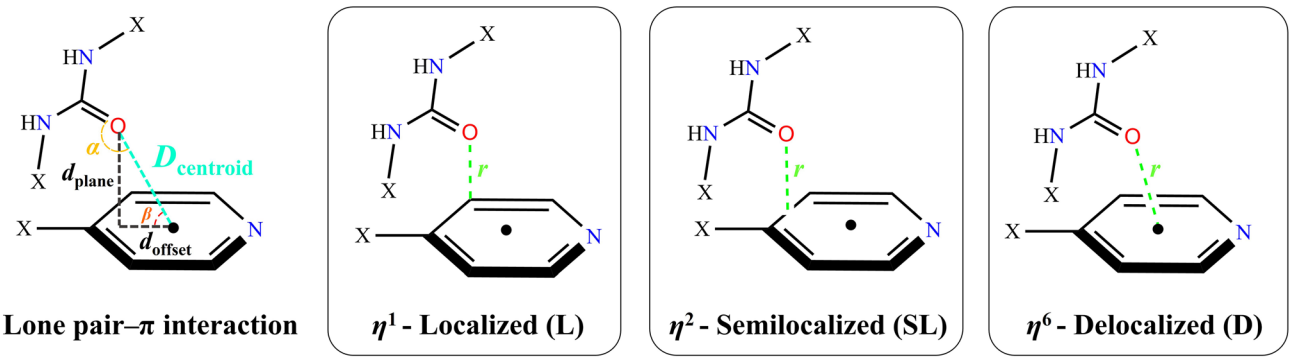

Scheme 2 Geometrical parameters[a] (left panel) and urea–C═O···π_{py} classification (right panel)[b].[89] [a] $D_{centroid}$ is the oxygen distance from the centroid of ring atoms. d_{plane} is the normal line from the oxygen to the ring plane. d_{offset} is the parameter which determines the displacement of oxygen from the center of the aromatic ring [$d_{offset} = (D_{centroid}^2 - d_{plane}^2)^{1/2}$]. [b] *r* is the shortest distance between the oxygen and ring member atom, centroid of bond or centroid of the ring atoms.

Table 6 Distances ($D_{centroid}$, d_{plane}, d_{offset}, *r*/Å) and angles (α, β/°) for the description of the lone pair–π interactions in **M-MeOH** and **M-EtOH** (M = Zn, Cd and Hg)[a]

Compounds	Interaction	$D_{centroid}$	d_{plane}	d_{offset}	α	β	*r*/atom(s)	Classification
Zn-MeOH	C═O···π_{py1}	3.565	3.338	1.25	97.11	69.44	3.349/C1–C4	η^2-SL
	C═O···π_{py2}	3.750	3.161	2.01	69.93	57.45	3.256/C7–C9	η^2-SL
Zn-EtOH	C═O···π_{py1}	3.565	3.338	1.25	97.50	69.44	3.349/C1–C4	η^2-SL
	C═O···π_{py2}	3.944	3.190	2.31	64.18	53.98	3.390/C7–C9	η^2-SL
Cd-MeOH	C═O···π_{py1}	3.507	3.315	1.14	97.67	70.95	3.335/C1–C4	η^2-SL
	C═O···π_{py2}	3.766	3.196	1.99	67.59	58.06	3.300/C7–C9	η^2-SL
Cd-EtOH	C═O···π_{py1}	3.516	3.329	1.13	98.16	71.22	3.338/C1–C4	η^2-SL
	C═O···π_{py2}	3.814	3.220	2.04	68.30	57.59	3.332/C7–C9	η^2-SL
Hg-MeOH	C═O···π_{py1}	3.462	3.305	1.03	96.27	72.67	3.323/C1–C4	η^2-SL
	C═O···π_{py2}	3.793	3.239	1.97	67.77	58.64	3.342/C7–C9	η^2-SL
Hg-EtOH	C═O···π_{py1}	3.503	3.376	0.93	95.58	74.52	3.405/C1–C4	η^2-SL
	C═O···π_{py2}	3.857	3.227	2.11	66.09	56.78	3.360/C7–C9	η^2-SL

[a] π_{py1}: N1–C1–C4–C5–C3–C2, π_{py2}: N4–C10–C9–C7–C8–C11.

oxygen and carbon atoms ($\sum R_{vdW}$ = 3.22 Å),[90] these interactions can be classified as semilocalized (η^2-SL) interaction.[91] In order to study of the urea–C═O···π_{py} interactions in more detail, we have conducted an extensive single-crystal X-ray crystallographic study on the Cambridge Structural Database (CSD)[92] with the help of ConQuest version 2024.1.0. This search focused on urea–C═O···π interactions and C···O contacts with a 4-substituted pyridyl ring in urea-based compounds. The processing of the obtained data allowed the recognition of several more examples of these intermolecular interactions (Fig. 5). In the CSD, 278 structures containing at least one urea–C═O group and a 4-substituted pyridyl ring have been identified. A detailed examination of the corresponding CIF files reveals that 47 structures (16.9% of the total) exhibit at least one lone pair–π interaction. In total, 118 lone pair–π contacts were identified.

Isostructurality of compounds

The similarity between all compounds with respect to their subassemblies or supramolecular constructs (SC) was exam-

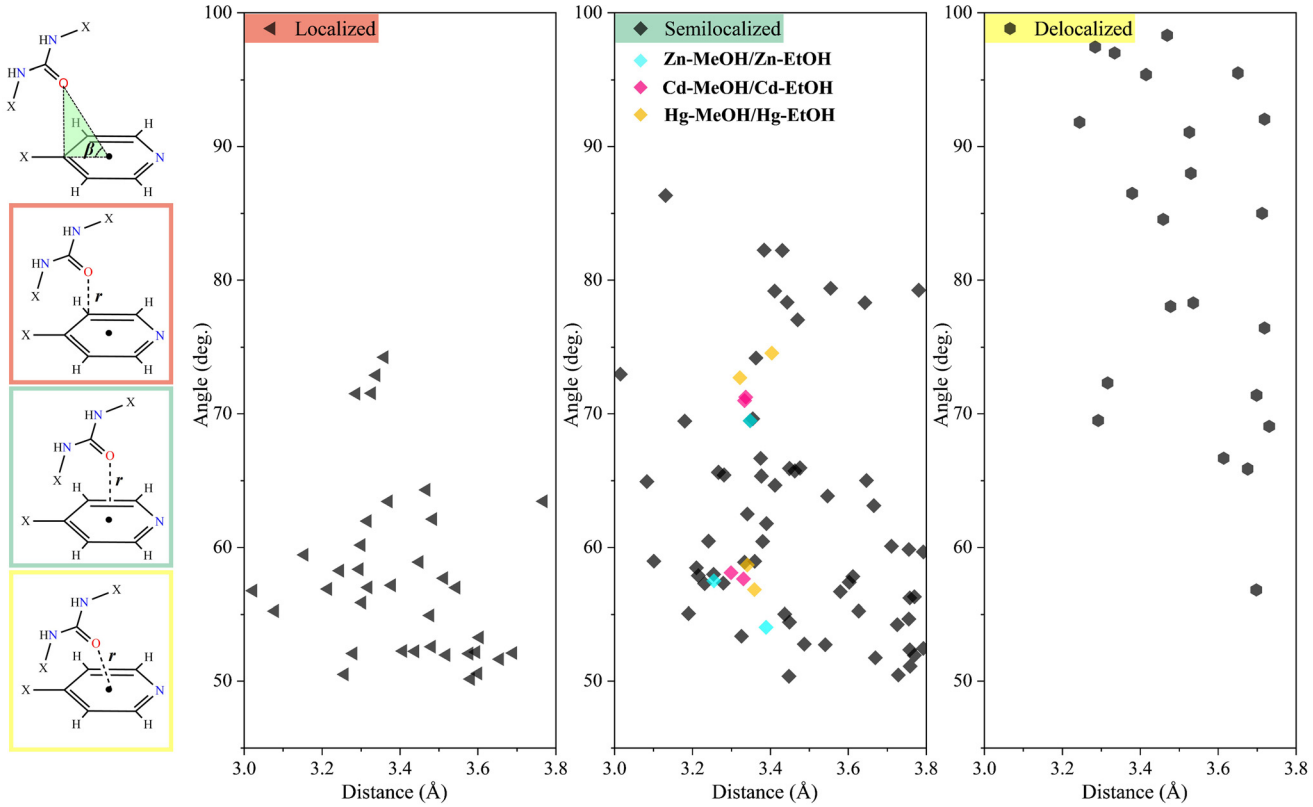

Fig. 5 An illustration of the search protocols. Scatter plots of the plane-centroid···O═C angle *versus* the shortest atom···O═C distance, bond-centroid···O═C distance and ring centroid···O═C distance that are in the acceptable range and extracted from the CSD data.

Table 7 Structural similarity (3D and 1D) parameters for the isostructural CPs

Combination		Dissimilarity index (X)	δa (°)	δp (°)	D (Å)
3D isostructurality	**Zn-MeOH & Zn-EtOH**	3.3	1.7	2.8	0.23
	Cd-MeOH & Cd-EtOH	2.1	1.0	1.8	0.13
	Hg-MeOH & Hg-EtOH	2.8	1.2	2.5	0.15
	Cd-MeOH & Hg-MeOH	2.2	0.8	2.0	0.03
	Cd-EtOH & Hg-EtOH	2.5	0.9	2.3	0.05
	Cd-MeOH & Hg-EtOH	2.9	1.2	2.7	0.17
	Cd-EtOH & Hg-MeOH	2.8	1.3	2.5	0.11
1D isostructurality	**Zn-MeOH & Cd-MeOH**	16.1	8.6	13.6	0.18
	Zn-MeOH & Hg-MeOH	16.8	8.9	14.1	0.20
	Zn-EtOH & Cd-EtOH	16.5	8.8	14.0	0.11
	Zn-EtOH & Hg-EtOH	17.4	9.1	14.8	0.14
	Zn-MeOH & Cd-EtOH	15.7	8.5	13.2	0.35
	Zn-MeOH & Hg-EtOH	16.5	8.8	13.9	0.37

ined using XPac 2.0.2 software introduced by Gelbrich and co-workers.[93–95] All the atomic coordinates (in crystal geometry) except the hydrogen atoms, were considered for the XPac analysis. Table 7 and Fig. 6 show the overall structural similarity among these six crystal structures. Supramolecular constructs are the subcomponents of crystal structures that have geo-

Compound	Zn-MeOH	Zn-EtOH	Cd-MeOH	Cd-EtOH	Hg-MeOH	Hg-EtOH
Zn-MeOH		3D	1D	1D	1D	1D
Zn-EtOH				1D		1D
Cd-MeOH				3D	3D	3D
Cd-EtOH					3D	3D
Hg-MeOH						3D
Hg-EtOH						

Fig. 6 Map showing the structural similarity (3D, 1D, and no similarity) for the six crystal structures. The gray color indicates a similar combination.

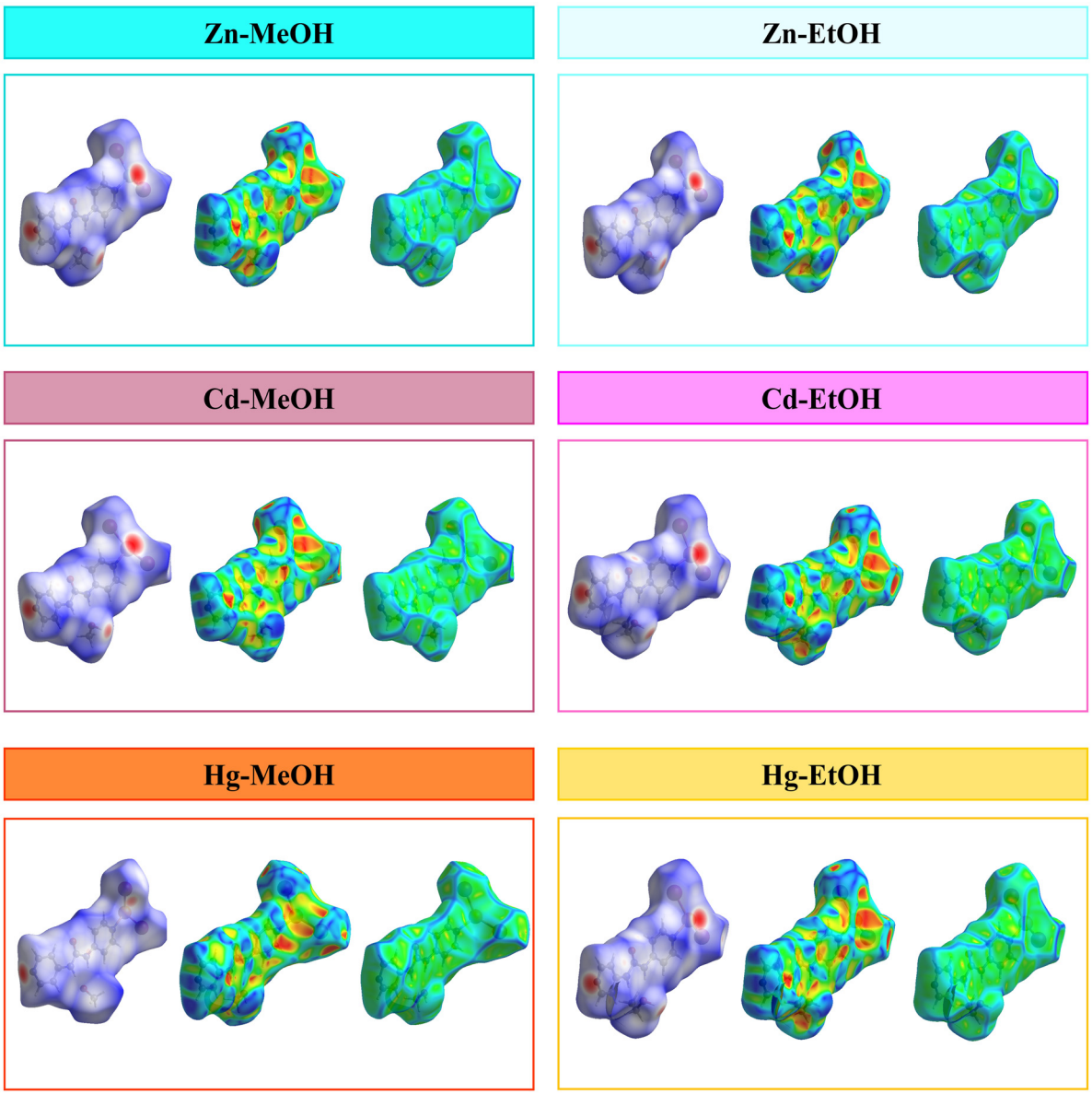

Fig. 7 Hirshfeld surfaces mapped with d_{norm} (left panel), shape index (middle panel) and curvedness (right panel) for the presented compounds.

metrical closeness with respect to the conformation and position of molecules. The comparison of the structures is merely based on the geometrical basis that takes account of angular, planar, and distance relationships between the kernel molecule (central molecule) and the cluster molecules (surrounding molecules) of a given coordination sphere of molecules generated around a central molecule by relative symmetry operations of the space group of each structure considered for comparison. The XPac dissimilarity index (X)[95] calculated for a coordination sphere comprising a kernel (central molecule) and other shell molecules shows 3D similarly between **Zn-MeOH** and **Zn-EtOH** with an (X) value of 3.3. The pertinent values of geometrical parameters *i.e.*, angles $[a]$ and planes $[p]$ used to calculate (X) for **Zn-MeOH** and **Zn-EtOH** are 1.7 and 2.8, respectively. Moreover, intriguing insights can be extracted from the Fig. S18 and S19.† In the plot of δp (°) *vs.* δa (°), more data points close to the origin (*i.e.*, data points at lower angles $[a]$) signify more similarity among the crystal structures. Thus, compound **Zn-MeOH** is more similar to compound **Zn-EtOH** than other compounds. Furthermore, when plotting (X)

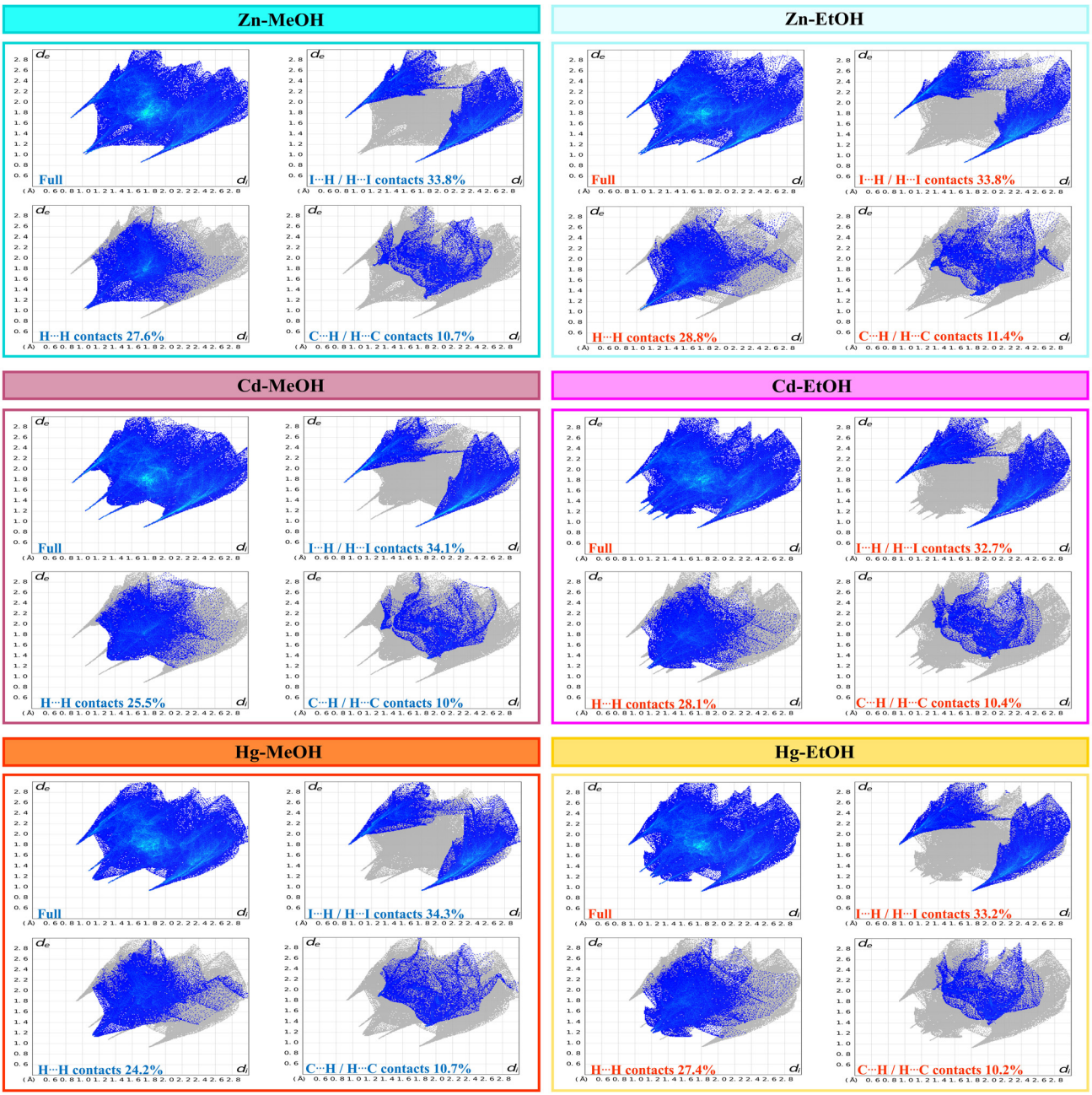

Fig. 8 Fingerprint plots of compounds, full and resolved into I···H/H···I, H···H, and C···H/H···C contacts showing the percentages of contacts contributing to the total Hirshfeld surface area of the molecules.

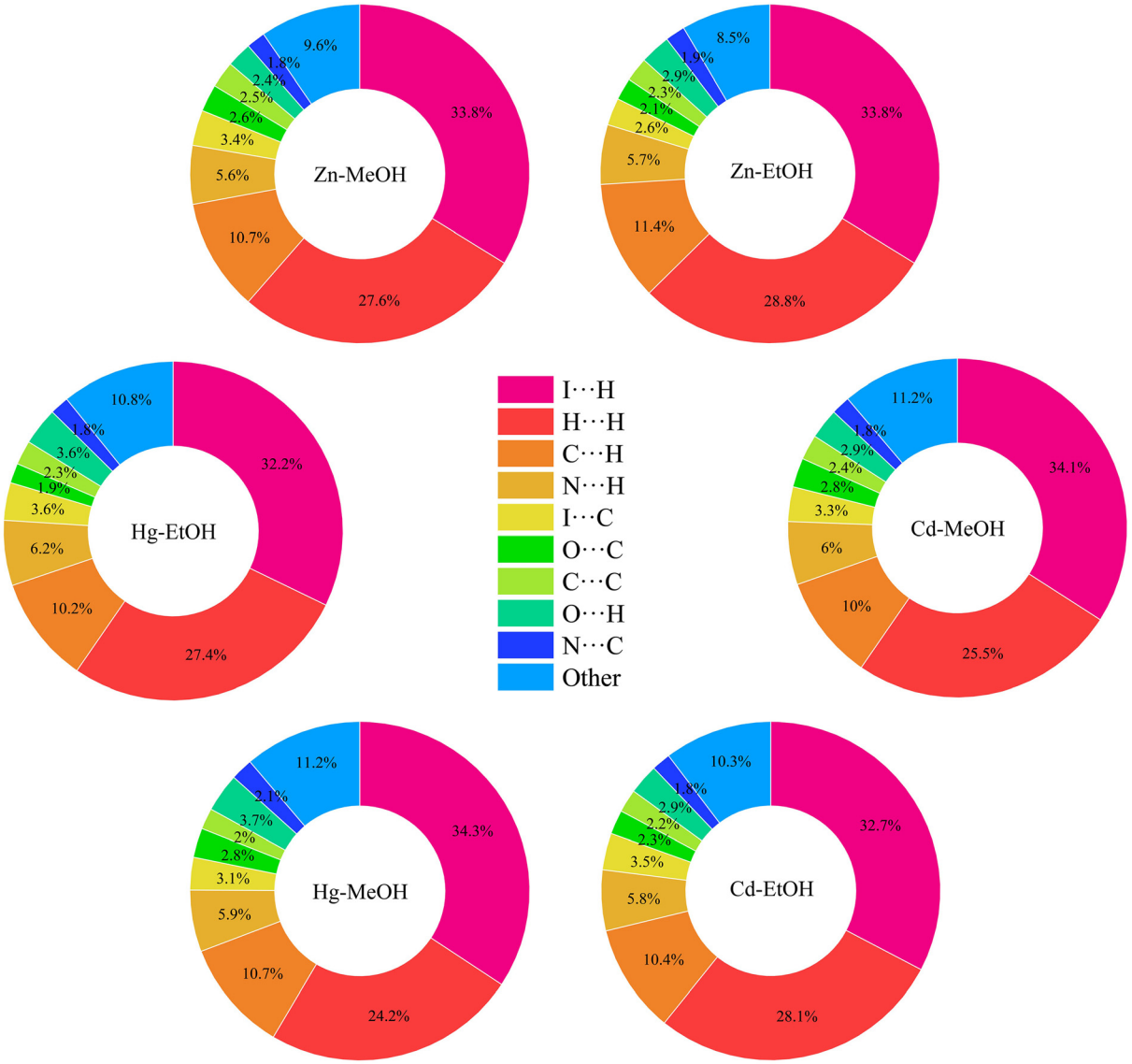

Fig. 9 The relative contribution of different intermolecular interactions to the Hirshfeld surface area in the presented compounds.

against δd (Å), it provides the stretching parameter 'D', which indicates the degree of elongation in one structure compared to another. A lower 'D' value signifies greater similarity, reinforcing the notion that compounds **Cd-MeOH** and **Hg-MeOH** exhibit significant structural resemblance, as illustrated in Table 7, Fig. S18 and S19.†

Analysis of Hirshfeld surfaces

In order to gain a comprehensive understanding of the strength and role of hydrogen bonds and other intermolecular interactions, and to assess their significance in maintaining the stability of the crystal lattice in all described crystals, we employed Hirshfeld surface analysis. These analyses serve to highlight the similarities and distinctions in the intermolecular interactions of the studied isostructural coordination polymers, shedding light on their structural relationships. Hirshfeld surface analysis and 2D fingerprint calculations were performed using Crystal Explorer[96] software, by importing the atomic coordinates from the CIF files. The distance from the nearest nucleus inside and outside the surface was measured and represented by the d_i and d_e, respectively, while a normalized contact distance was represented as d_{norm}. The white, red, and blue colors are selected for the visualization of the d_{norm} function with very high resolution. The Hirshfeld surface analysis of compounds is illustrated in Fig. 7, showing surfaces that have been mapped over the d_{norm} range of −0.7 to 1.6 Å, shape index (−1.0 to 1.0 Å) and curvedness (−4.0 to 0.4 Å). The deep red circular depressions on the d_{norm} surfaces indicate hydrogen bond interactions, which are notably present in the crystal structures of all compounds. The analysis reveals that in the crystal structure of all compounds the I···H hydrogen bonds are the dominant intermolecular

interactions (the highest contributor to the Hirshfeld surface area). Also, in agreement with the geometrical analysis, it is found that the iodine atoms in all compounds are involved in X–H···I (X = C and O) hydrogen bonding interactions (Tables 3–5 and Fig. 4). The H···H intermolecular interaction is observed as a small spike, which makes the second most significant contribution to the total Hirshfeld surfaces. In addition, the presence of relatively weak C···H/H···C interactions is observed (Fig. 8 and 9).

FT-IR spectra

The infrared absorption (FT-IR) spectra of the **4bpu** ligand and **M-MeOH** and **M-EtOH** compounds (M = Zn, Cd and Hg) were obtained using the KBr pellet (Fig. S2–S8, ESI†). All compounds exhibit vibrations related to C=C aromatic, C=O urea, N–H urea and C–H groups. Upon examining the FT-IR spectrum, we find that the stretching vibrational frequency of the C=O group in all compounds is sharp and changes from 1735 to 1742 cm^{-1}. The absorption peaks at 1588–1596 cm^{-1} belong to the bending vibration peak of urea N–H groups. Above 3000 cm^{-1}, stretching vibrational frequencies of the N–H of the urea group fall between 3200 and 3523 cm^{-1} and those of C–H aromatic range from 3045 to 3091 cm^{-1}, appearing as a weak peak.[18,97,98] Since MeOH and EtOH molecules are removed from the structure of these compounds after grinding, the ATR-FTIR spectra were analyzed to enable sample preparation without the grinding step. As shown in Fig. S20,† the differences in the stretching vibrational frequencies of the C–O bonds in MeOH and EtOH clearly distinguish between the FT-IR spectrum of **M-MeOH** and **M-EtOH** compounds (M = Zn, Cd and Hg).[99]

Powder X-ray diffraction (PXRD) and thermogravimetric analysis (TGA)

To confirm the phase purity of all compounds, the PXRD patterns have been recorded at room temperature. The diffraction peaks of the as-synthesized samples are in agreement with the simulated data, indicating the phase purity of the synthesized compounds (Fig. S21 and S22†). Moreover, as shown in Fig. S23,† the isostructurality of these compounds is confirmed based on comparison of the simulated PXRD patterns from the X-ray single-crystal data. The thermal stability of compounds has been investigated through thermogravimetric analysis (TGA), exhibiting similar decomposition patterns (Fig. S24†). The comparable weight loss patterns observed in the TGA curves of the **Zn-MeOH**/**Zn-EtOH**, **Cd-MeOH**/**Cd-EtOH** and **Hg-MeOH**/**Hg-EtOH** imply similar decomposition pathways. However, the distinct percentage of weight loss for each compound indicates a difference in the stability of their frameworks. It is plausible that variations in the nature of bonding or the strength of intermolecular forces within the structures may contribute to the dissimilar thermal behaviors. Table S3† presents the temperature range, along with the calculated and observed weight loss percentages for methanol and ethanol guest molecules.

Conclusion

In summary, this work demonstrates a systematic investigation of the synthesis of six structurally identical Zn^{II}, Cd^{II} and Hg^{II} pseudopolymorphic urea-based coordination polymers. The crystal structure determination by SC-XRD of these isostructural coordination polymers revealed one-dimensional zig-zag chains. The expected bifurcated hydrogen bonds between urea groups, typically forming an α-tape motif, were absent in these structures. Instead, the coordination polymers exhibit a unique arrangement where robust and repetitive hydrogen bonds between the urea groups and solvent molecules (MeOH or EtOH) connect the chains, forming a distinctive supramolecular network. Additional interactions, including urea–C=O···π_{py} (lone pair–π) and C–H···I hydrogen bonding, contribute to stabilizing the crystal structure. This work is one of the few systematic studies that comprehensively examines the aspect of controlling pseudopolymorphism *via* supramolecular interactions. These findings highlight the significant role of solvent interactions in supramolecular assemblies, extend the understanding of pseudopolymorphism and provide insights for designing materials with tailored intermolecular interactions.

Author contributions

Ghazale Khorshidi: investigation, formal analysis, writing – original draft, software, and writing – review & editing. Behrouz Notash: conceptualization, supervision, funding acquisition, project administration, writing – review & editing, and software.

Data availability

The authors confirm that the data supporting the findings of this study are available within the article and its ESI.†

Conflicts of interest

There are no conflicts to declare.

Acknowledgements

The authors thank the Graduate Study Councils of Shahid Beheshti University, G. C. for financial support. We are thankful to Dr Alireza Salimi (Ferdowsi University of Mashhad) for his help in crystallographic part.

References

1 S. Bhattacharyya and T. K. Maji, *Coord. Chem. Rev.*, 2022, **469**, 214645.

2 S. A. A. Razavi and A. Morsali, *Coord. Chem. Rev.*, 2019, **399**, 213023.
3 N. Li, R. Feng, J. Zhu, Z. Chang and X.-H. Bu, *Coord. Chem. Rev.*, 2018, **375**, 558–586.
4 Y. Li, Y. Wang, W. Fan and D. Sun, *Dalton Trans.*, 2022, **51**, 4608–4618.
5 D.-X. Xue, Q. Wang and J. Bai, *Coord. Chem. Rev.*, 2019, **378**, 2–16.
6 A. Bavykina, N. Kolobov, I. S. Khan, J. A. Bau, A. Ramirez and J. Gascon, *Chem. Rev.*, 2020, **120**, 8468–8535.
7 K. Biradha, A. Goswami and R. Moi, *Chem. Commun.*, 2020, **56**, 10824–10842.
8 J.-Q. Liu, Z.-D. Luo, Y. Pan, A. K. Singh, M. Trivedi and A. Kumar, *Coord. Chem. Rev.*, 2020, **406**, 213145.
9 L. Chen, D. Liu, J. Peng, Q. Du and H. He, *Coord. Chem. Rev.*, 2020, **404**, 213113.
10 Y. Feng, Y. Wang and Y. Ying, *Coord. Chem. Rev.*, 2021, **446**, 214102.
11 A. E. Thorarinsdottir and T. D. Harris, *Chem. Rev.*, 2020, **120**, 8716–8789.
12 Q. Zhao, Q. Y. Li and J. Li, *CrystEngComm*, 2022, **24**, 6751–6761.
13 J. Wang, N. N. Chen, C. Zhang, L. Y. Jia and L. Fan, *CrystEngComm*, 2020, **22**, 811–820.
14 Z. Zhang, W. Sang, L. Xie and Y. Dai, *Coord. Chem. Rev.*, 2019, **399**, 213022.
15 R. M. Safdar, H. Ali and Z. Li, *Molecules*, 2022, **27**, 100.
16 S. Mondal and P. Dastidar, *Cryst. Growth Des.*, 2020, **20**, 7411–7420.
17 A. Karmakar, S. Hazra and A. J. L. Pombeiro, *Coord. Chem. Rev.*, 2022, **453**, 214314.
18 P. Biswas and P. Dastidar, *Inorg. Chem.*, 2021, **60**, 3218–3231.
19 R. Brahma and J. B. Baruah, *CrystEngComm*, 2021, **23**, 3812–3827.
20 S. Glomb, D. Woschko, G. Makhloufi and C. Janiak, *ACS Appl. Mater. Interfaces*, 2017, **9**, 37419–37434.
21 J. M. Roberts, B. M. Fini, A. A. Sarjeant, O. K. Farha, J. T. Hupp and K. A. Scheidt, *J. Am. Chem. Soc.*, 2012, **134**, 3334–3337.
22 A. Azhdari Tehrani, L. Esrafili, S. Abedi, A. Morsali, L. Carlucci, D. M. Proserpio, J. Wang, P. C. Junk and T. Liu, *Inorg. Chem.*, 2017, **56**, 1446–1454.
23 L. Esrafili, M. Gharib and A. Morsali, *Dalton Trans.*, 2019, **48**, 17831–17839.
24 A. M. Cheplakova, D. G. Samsonenko, V. A. Lazarenko, P. V. Dorovatovskii, Y. V. Zubavichus, V. N. Khrustalev, M. I. Rakhmanova and V. P. Fedin, *CrystEngComm*, 2022, **24**, 2057–2071.
25 H. Moon, S. W. Lim, D. Kim, O.-S. Jung and Y.-A. Lee, *CrystEngComm*, 2021, **23**, 1272–1280.
26 B. Moulton and M. J. Zaworotko, *Chem. Rev.*, 2001, **101**, 1629–1658.
27 A. Karmakar, A. Paul and A. J. L. Pombeiro, *CrystEngComm*, 2017, **19**, 4666–4695.
28 G. Khorshidi and B. Notash, *Sci. Rep.*, 2024, **14**, 27586.
29 P. Cui, J. Wu, X. Zhao, D. Sun, L. Zhang, J. Guo and D. Sun, *Cryst. Growth Des.*, 2011, **11**, 5182–5187.
30 B. Notash and B. Rezaei Kheirkhah, *New J. Chem.*, 2018, **42**, 15014–15021.
31 W.-W. Dong, D.-S. Li, J. Zhao, L.-F. Ma, Y.-P. Wu and Y.-P. Duan, *CrystEngComm*, 2013, **15**, 5412–5416.
32 B. Notash, *J. Mol. Struct.*, 2018, **1156**, 534–543.
33 B. Notash, B. Rezaei Kheirkhah and G. Khorshidi, *J. Mol. Struct.*, 2023, **1294**, 136324.
34 S. S. Nagarkar, A. K. Chaudhari and S. K. Ghosh, *Cryst. Growth Des.*, 2012, **12**, 572–576.
35 H. Ju, Y. Habata and S. S. Lee, *Cryst. Growth Des.*, 2020, **20**, 4640–4648.
36 J. J. Wu, W. Xue, M. L. Cao, Z. P. Qiao and B. H. Ye, *CrystEngComm*, 2011, **13**, 5495–5501.
37 A. B. Lago, R. Carballo, S. Rodríguez-Hermida and E. M. Vázquez-López, *CrystEngComm*, 2013, **15**, 1563–1570.
38 M.-L. Han, X.-H. Chang, X. Feng, L.-F. Ma and L.-Y. Wang, *CrystEngComm*, 2014, **16**, 1687–1695.
39 E. Lee, J.-Y. Kim, S. S. Lee and K.-M. Park, *Chem. – Eur. J.*, 2013, **19**, 13638–13645.
40 L. Dobrzańska, *Inorg. Chem. Commun.*, 2015, **55**, 21–24.
41 H. Wang, J. Yang and T. C. W. Mak, *New J. Chem.*, 2014, **38**, 4690–4695.
42 L. K. Das, A. M. Kirillov and A. Ghosh, *CrystEngComm*, 2014, **16**, 3029–3039.
43 K. M. Fromm, J. L. S. Doimeadios and A. Y. Robin, *Chem. Commun.*, 2005, 4548–4550.
44 V. S. S. Kumar, F. Christopher Pigge and N. P. Rath, *New J. Chem.*, 2003, **27**, 1554–1556.
45 J.-P. Zhang, X.-C. Huang and X.-M. Chen, *Chem. Rev.*, 2009, **38**, 2385–2396.
46 B. Notash, M. Farhadi Rodbari and M. Kubicki, *ACS Omega*, 2023, **8**, 13140–13152.
47 B. Notash, M. Farhadi Rodbari, G. Gallo and R. Dinnebier, *Inorg. Chem.*, 2021, **60**, 9212–9223.
48 J. L. Atwood and J. W. Steed, *Encyclopedia of Supramolecular Chemistry*, M. Dekker, 2004.
49 H. G. Brittain, *J. Pharm. Sci.*, 2012, **101**, 464–484.
50 P. Lu and S. Rohani, *Curr. Med. Chem.*, 2009, **16**, 884–905.
51 K. J. Chavez, M. Guevara and R. W. Rousseau, *Cryst. Growth Des.*, 2010, **10**, 3372–3377.
52 G. Kang, Y. Jeon, K. Y. Lee, J. Kim and T. H. Kim, *Cryst. Growth Des.*, 2015, **15**, 5183–5187.
53 Z. Li, J. Zhou, K. Zhang, Y. Zhang, S. Wu and J. Gong, *Cryst. Growth Des.*, 2022, **22**, 5322–5334.
54 H. R. Khavasi and B. Mir Mohammad Sadegh, *Cryst. Growth Des.*, 2012, **12**, 4798–4804.
55 R. Thakuria, N. K. Nath, S. Roy and A. Nangia, *CrystEngComm*, 2014, **16**, 4681–4690.
56 J. Galcera, T. Friščić, E. Molins and W. Jones, *CrystEngComm*, 2013, **15**, 1332–1338.
57 J. Galcera, T. Friščić, K. E. Hejczyk, L. Fábián, S. M. Clarke, G. M. Day, E. Molins and W. Jones, *CrystEngComm*, 2012, **14**, 7898–7906.

58 B. K. Saha and A. Nangia, *Heteroat. Chem.*, 2007, **18**, 185–194.
59 G. Khorshidi, B. Notash and M. Kubicki, *CrystEngComm*, 2024, **26**, 4082–4097.
60 A. Kalman, *Acta Crystallogr., Sect. B:Struct. Sci.*, 2005, **61**, 536–547.
61 L. Fábián and A. Kámán, *Acta Crystallogr., Sect. B:Struct. Sci.*, 2004, **60**, 547–558.
62 J. Kendrick, R. Montis, M. B. Hursthouse and F. J. J. Leusen, *Cryst. Growth Des.*, 2013, **13**, 2906–2915.
63 G. R. Desiraju, *Angew. Chem., Int. Ed. Engl.*, 1995, **34**, 2311–2327.
64 S. K. Nayak, M. K. Reddy, T. N. Guru Row and D. Chopra, *Cryst. Growth Des.*, 2011, **11**, 1578–1596.
65 A. Singh, A. Ramanan and D. Bandyopadhyay, *Cryst. Growth Des.*, 2011, **11**, 2743–2754.
66 Y. Zhao, H. Wu, T. J. Emge, Q. Gong, N. Nijem, Y. J. Chabal, L. Kong, D. C. Langreth, H. Liu, H. Zeng and J. Li, *Chem. – Eur. J.*, 2011, **17**, 5101–5109.
67 Y.-F. Han, W.-G. Jia, W.-B. Yu and G.-X. Jin, *Chem. Soc. Rev.*, 2009, **38**, 3419–3434.
68 Y.-F. Han, W.-G. Jia, Y.-J. Lin and G.-X. Jin, *Angew. Chem., Int. Ed.*, 2009, **48**, 6234–6238.
69 J. S. Geng, W. Feng, J. Li, X. Y. Tang, L. Meng, J. P. Yu, K. Q. Hu, L. H. Yuan, L. Mei and W. Q. Shi, *Inorg. Chem.*, 2022, **61**, 10694–10704.
70 H. H. Wang, Y. Zhang, D. B. Yang, L. Hou, Z. Y. Li and Y. Y. Wang, *Cryst. Growth Des.*, 2021, **21**, 2488–2497.
71 S. Chand, S. Hota, S. M. Elahi and M. C. Das, *Polyhedron*, 2018, **153**, 115–121.
72 B. Bhattacharya, D. K. Maity, R. Mondal, E. Colacio and D. Ghoshal, *Cryst. Growth Des.*, 2015, **15**, 4427–4437.
73 A. H. Chughtai, N. Ahmad, H. A. Younus, A. Laypkov and F. Verpoort, *Chem. Soc. Rev.*, 2015, **44**, 6804–6849.
74 W. Zhou, H. Wu and T. Yildirim, *J. Am. Chem. Soc.*, 2008, **130**, 15268–15269.
75 S. R. Caskey, A. G. Wong-Foy and A. J. Matzger, *J. Am. Chem. Soc.*, 2008, **130**, 10870–10871.
76 X. Y. Tian, H. L. Zhou, X. W. Zhang, C. Wang, Z. H. Qiu, D. D. Zhou and J. P. Zhang, *Inorg. Chem.*, 2020, **59**, 6047–6052.
77 Z. U. Nisa, L. Tashi, C. Sen, N. A. Ashashi, S. C. Sahoo and H. N. Sheikh, *New J. Chem.*, 2020, **44**, 8125–8137.
78 G. Liu, Y. K. Lu, Y. Y. Ma, X. Q. Wang, L. Hou and Y. Y. Wang, *Dalton Trans.*, 2019, **48**, 13607–13613.
79 B. Dutta, A. Dey, K. Naskar, S. Maity, F. Ahmed, S. Islam, C. Sinha, P. Ghosh, P. P. Ray and M. H. Mir, *New J. Chem.*, 2018, **42**, 10309–10316.
80 S. K. Chandran, N. K. Nath, S. Cherukuvada and A. Nangia, *J. Mol. Struct.*, 2010, **968**, 99–107.
81 G. Mahmoudi, A. Morsali, A. D. Hunter and M. Zeller, *CrystEngComm*, 2007, **9**, 704–714.
82 L. Yang, D. R. Powell and R. P. Houser, *Dalton Trans.*, 2007, 955–964.
83 J.-Y. Cheng, F.-W. Ding, P. Wang, C.-W. Zhao and Y.-B. Dong, *ChemPlusChem*, 2016, **81**, 743–751.
84 B. Notash, N. Safari and H. R. Khavasi, *CrystEngComm*, 2012, **14**, 6788–6796.
85 B. Notash, N. Safari and H. R. Khavasi, *Inorg. Chem.*, 2010, **49**, 11415–11420.
86 X. F. Wang, Y. Lv, T. A. Okamura, H. Kawaguchi, G. Wu, W. Y. Sun and N. Ueyama, *Cryst. Growth Des.*, 2007, **7**, 1125–1133.
87 M. C. Etter, *Acc. Chem. Res.*, 1990, **23**, 120–126.
88 M. C. Etter, J. C. MacDonald and J. Bernstein, *Acta Crystallogr., Sect. B:Struct. Sci.*, 1990, **46**, 256–262.
89 B. Ebrahimi, B. Notash, T. Matar and R. Dinnebier, *Inorg. Chem.*, 2024, **63**, 983–999.
90 A. Bondi, *J. Phys. Chem. C*, 1964, **68**, 441–451.
91 T. J. Mooibroek, P. Gamez and J. Reedijk, *CrystEngComm*, 2008, **10**, 1501–1515.
92 C. R. Groom, I. J. Bruno, M. P. Lightfoot and S. C. Ward, *Acta Crystallogr., Sect. B:Struct. Sci., Cryst. Eng. Mater.*, 2016, **72**, 171–179.
93 T. Gelbrich and M. B. Hursthouse, *CrystEngComm*, 2005, **7**, 324–336.
94 T. Gelbrich and M. B. Hursthouse, *CrystEngComm*, 2006, **8**, 448–460.
95 F. P. A. Fabbiani, B. Dittrich, A. J. Florence, T. Gelbrich, M. B. Hursthouse, W. F. Kuhs, N. Shankland and H. Sowa, *CrystEngComm*, 2009, **11**, 1396–1406.
96 S. K. Wolff, D. J. Grimwood, J. J. McKinnon, M. J. Turner, D. Jayatilaka and M. A. Spackman, *CrystalExplorer, Version 3.1*, University of Western Australia, Australia, 2012.
97 S. Banerjee, D. P. Kumar, S. Bandyopadhay, N. N. Adarsh and P. Dastidar, *Cryst. Growth Des.*, 2012, **12**, 5546–5554.
98 U. Manna, S. Kayal, B. Nayak and G. Das, *Dalton Trans.*, 2017, **46**, 11956–11969.
99 T. Coldea, C. Socaciu, F. Fetea, F. Ranga, R. Pop and M. Florea, *Not. Bot. Horti Agrobot.*, 2013, **41**, 143–149.